Sensors & Transducers, Vol. 18, Special Issue, January 2013, pp. 24-32

www.sensorsportal.com

Sensors & Transducers

ISSN 1726-5479

http://www.sensorsportal.com

Atmospheric Icing Sensors - Capacitive Techniques

[1] Umair N. Mughal, Muhammad S. Virk
Narvik University College, Narvik-8505, Norway
[1] Tel.: +4776966372, +4776966810
E-mail: unm@hin.no

Received: 30 October 2012 /Accepted: 14 December 2012 /Published: 22 January 2013

Abstract: The application of capacitive sensing technique is widely distributed in different physical domains primarily because of the diversity in dielectric permittivity and due to its minimum loading error and inertial effects. Atmospheric ice is a complex mixture of water, ice and air which is reflected in its complex dielectric constant. There are many existing atmospheric icing sensors but only few are based on their complex dielectric permittivity measurements. This technique is very suitable because the capacitive variation in this mixture is due to the reorientation of water dipole in the electromagnetic radiation's oscillating field. Depending on the frequency, the dipole may move in time to the field, lag behind it or remain apparently unaffected. This variation is clearly reflected on the Cole-Cole-diagram, which is a measure of the relaxation frequency. This paper is a detailed understanding of some capacitive sensing techniques in general but based upon dielectric variations and some existing capacitive based atmospheric ice sensing techniques. It is emphasized that the capacitive method proposed by Jarvenin provides maximum atmospheric icing parameters hence future atmospheric icing sensors may utilize the proposed technique with some modifications to further reduce the loading errors. *Copyright © 2013 IFSA.*

Keywords: Atmospheric ice, Relaxation frequency, Debye relation, Dielectric, Capacitance.

1. Introduction

Atmospheric icing is the term used to describe the accretion of ice on structures or objects under certain conditions. This accretion can take place either due to freezing precipitation or freezing fog. It depends mainly on the shape of the object, wind speed, temperature, liquid water content (amount of liquid water in a given volume of air) and droplet size distribution (conventionally known as the median volume diameter). The major *effects of atmospheric icing* on structure are the static ice loads, wind action on iced structure and dynamic effects.

Generally an icing event is defined as period of the time when the temperature is below 0 °C and the relative humidity is above 95 %. Ice accretion can be defined as, *any process of ice build up and snow accretion on the surface of objects exposed to the atmosphere* [1]. Atmospheric icing is traditionally classified according to two different processes (see Fig. 1.), which are [1]:

i. Precipitation icing;
ii. In-cloud icing.

Fig. 2 shows the type of accreted ice as a function of wind speed and temperature. In this figure, the curve shifts to the left with the increasing liquid water content and with decreasing object size. A classification of atmospheric ice is shown in Table 1.

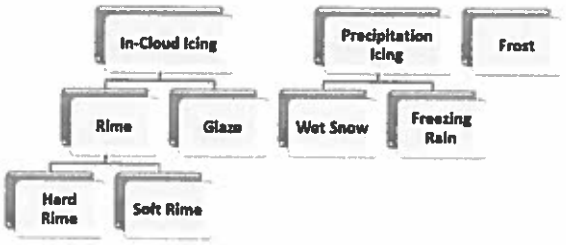

Fig. 1. Ice Types [1].

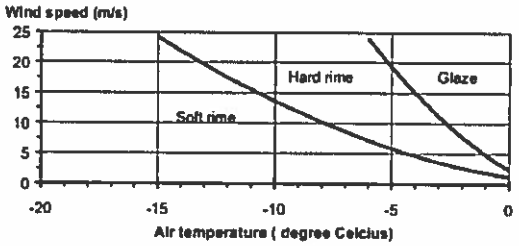

Fig. 2. Atmospheric ice as a function of wind speed and ambient temperature [1].

Table 1. Typical Properties of Accreted Atmospheric Ice [1].

Type of ice	Density (kg/m^3)	General Appearance	
		Color	Shape
Glaze	900	Transparent	Evenly distributed / icicles
Wet Snow	300-600	White	Evenly distributed / eccentric
Hard Rime	600-900	Opaque	Eccentric, pointing windward
Soft Rime	200-600	White	Eccentric, pointing windward

1.2. Atmospheric Icing Sensors

A robust technique to detect icing and ice accretion rates has not yet been reported in the published literature. It is a challenging task to devise a measurement technique that can deal with both rime and glaze icing and can measure icing rate, load and duration without being affected by the icing event. Currently, all the ice detectors available are capable of measuring either one or both phenomenon such as detecting the icing event and measuring the rate of icing. As ice sensors can be integrated with ice mitigation systems, it is important for these sensors to deliver the necessary information timely enough so as to be able to operate anti-icing and de-icing mitigation strategies effectively. To distinguish between snow and ice can be considered to be an important factor for the determination of deicing power requirements. Hence, measurement of an icing event or related phenomena bounds a set of requirements which include the ability of a sensor/probe to detect icing with high sensitivity without being influenced by the icing incident. Icing measurement techniques can be classified into direct and indirect methods as follows:

1.2.1. Indirect Methods

The indirect methods of ice detection involve measuring weather conditions such as humidity, and temperature that lead to icing or detecting the effects of icing, for example, reduction in the power generated by the wind turbine, reduction in the speed of anemometers or measuring the variables that cause icing or variables that correlate with the occurrence of icing, such as cloud height and visibility [2]. Empirical or deterministic models are then used to determine when icing is occurring. Also Homola et. al. [3] have outlined five indirect measurement methods. The reduction in the speeds of anemometers method of Craig and Craig [4] and the noise generation frequency method of Seifert [5] are typical examples of indirect methods.

1.2.2. Direct Methods

The direct methods of ice and snow detection are based on the principle of detecting property changes caused by accretion such as mass, dielectric constants, conductivities, or inductance. Although Homola et. al. [3] outlined twenty four direct measurement methods but they still need to be more categorized for further exploration. For more details on all of these categories see [6]. The categorization of these direct methods can be:

i. Capacitive techniques;
ii. Microwave techniques;
iii. Inductance techniques;
iv. Ultrasonic techniques;
v. Acoustic techniques;
vi. Infrared techniques;
vii. Resonance techniques.

2. Capacitive Sensing Technique - In General

From the above categories, the capacitive technique is the main focus of this review. The capacitance depends on the geometrical arrangement of the conductors and on the dielectric material between them, $C=C(\varepsilon, G)$. For example, for a capacitor formed by n equal parallel plane plates having a geometry G depending upon area A, with a distance d between each pair, and an interposed material with a relative dielectric constant ε_r, the capacitance is

$$C = \varepsilon_0 \varepsilon_r \frac{A}{d}(n-1), \quad (1)$$

where ε_o = 8.85 pF/m is the dielectric constant for vacuum. Therefore, any quantity producing a variation in ε_r, A, or d will result in the change in the capacitance C and can be in principle sensed by that device.

2.1. Dielectric Constant from Electronic Polarization

The electron orbiting a nucleus is like a harmonic oscillation with a natural frequency ω_o mentioned in Kao [7]. The dynamic equation can be defined as,

$$m\frac{d^2\Delta x}{dt^2} = -\gamma\Delta x - ZqF_{loc}, \tag{2}$$

where Δx is the electrons displacement, m is the electron mass, q is the electronic charge, Z is the number electrons involved, F_{loc} is the local field acting on the atoms, and γ is the force constant. Also the natural oscillation frequency is given as, $\omega_o = \sqrt{\gamma/m}$

The oscillating electron is equivalent to an electric dipole and would radiate energy according to electromagnetic theory of radiation. This energy can be taken as a damping mechanism and $\beta\, dx/dt$ is a retarding force, hence our dynamic equation is,

$$m\frac{d^2\Delta x}{dt^2} + m\omega_o^2\Delta x = -\beta\frac{dx}{dt} - ZqF_{loc} \tag{3}$$

From Bohr's Model, we have the potential of electron given as,

$$E = \hbar\omega_o = \frac{mq^4}{(4\pi\varepsilon_o)^2\hbar^2} \tag{4}$$

where $\hbar = h/2\pi$ and h is the Plank's constant. Also when $Z=1$ we have electronic polarization, $\alpha_e = 4\pi\varepsilon_o R^3$ where R is the radius of the ground state orbit of Bohr's atom. Similarly, electronic susceptibility and dielectric constant is given as,

$$\chi_e = \frac{N\alpha_e}{\varepsilon_o} = \frac{N}{\varepsilon_o}\left[\frac{(Zq)^2}{m\omega_o^2}\right]$$
$$\varepsilon_r = 1 + \chi_e = 1 + \frac{N}{\varepsilon_o}\left[\frac{(Zq)^2}{m\omega_o^2}\right] \tag{5}$$

2.2. Complex Dielectric Constant

When a time varying electric field is applied across a parallel plate capacitor with the plate area of one unit and a separation of d between the plates, then the total current is given by:

$$J_T = J + \frac{dD}{dt} = J + \varepsilon^*\frac{dF}{dt}, \tag{6}$$

where J is the conduction current and ε^* is the complex permittivity which is introduced to allow for dielectric losses due to friction accompanying polarization and orientation of electric dipoles. Mathematically,

$$\varepsilon^* = \varepsilon' - j\varepsilon'' = \left(\varepsilon_r' - j\varepsilon_r''\right)\varepsilon_o, \tag{7}$$

where ε_r' is the dielectric storage constant and ε_r'' is the dielectric loss factor. Similarly loss tangent is defined as, $\tan\delta = \varepsilon_r''/\varepsilon_r'$ where δ is the loss angle. We can use the instantaneous energy absorbed per second per cubic centimeter is given by $J_T(t)F(t)$. Thus, on average, the amount of energy per second per cubic centimeter absorbed by the material is

$$W = \omega\varepsilon_r''\varepsilon_o F_m^2/2 \tag{8}$$

The discrete nature of matter, and the behavior and interaction of those particles, can be manifested through their response to time varying electric fields with wavelengths comparable the distances between the particles. To measure the dynamic response, we can use either use *time domain approach* or *frequency domain approach*. From the viewpoint of measuring techniques, the time domain approach is simpler than the frequency domain approach, but from the viewpoint of data analysis, the time domain approach is more complex. However, both approaches should be intimately connected and should yield, in principle, the same results.

2.2.1. Time Domain Approach

In this we measure the time dependent polarization immediately after the application of a step function electric field or we measure the decay of the polarization from an initial steady state value to zero after the sudden removal of an initial polarizing field. This decay is generally referred to as *dielectric relaxation*. This approach provides conspicuous information about the nonlinearity of the dielectric behavior simply by varying the amplitude of the applied step function held. Experimental arrangement for the measurements of the time domain response (i.e., the transient charging or discharging current, resulting from the application or the removal of a step DC voltage) is given in Fig. 3.

In this circuit, the switch S_1 has 2 positions: one for turning on the step DC voltage to start the flow of charging current, the other for short circuiting the specimen to allow the discharging current to flow after the specimen has been fully charged to a steady state level. The switch S_2 is used to short circuit R_1 to provide a path for surge currents for a very short

period of time to protect the circuit; it also gives a chance to adjust the amplifier to a null position before recording the transient current. It is important to make the time constant of the amplifier which depends on the stray capacitance in shunt with R_1, much smaller than the time during which the transient current is flowing. The specimen has the guard and the guarded electrodes, the outer guard electrode being connected to ground to eliminate surface leakage currents from the specimen. The charging or discharging current is measured as a voltage appearing across R_1 by means of a DC amplifier. The voltage drop from point A to ground is made zero by a negative feedback in the amplifier circuit, which produces a voltage across R_2 equal and opposite to that across R_1 thus making the applied step voltage across the specimen only. The step voltage and the charging and discharging current as a function of time are also shown in Fig. 4 in which I_o is the steady DC component of the charging current and the width of the step voltage is 63 seconds.

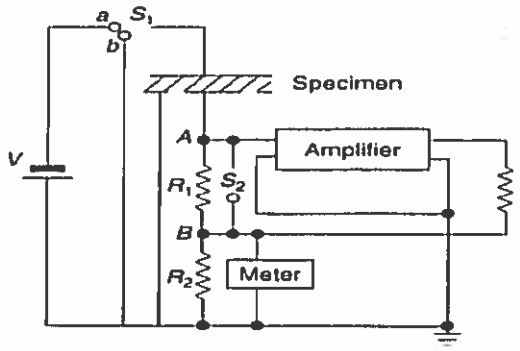

Fig. 3. Experimental arrangement for measuring relaxation time [7].

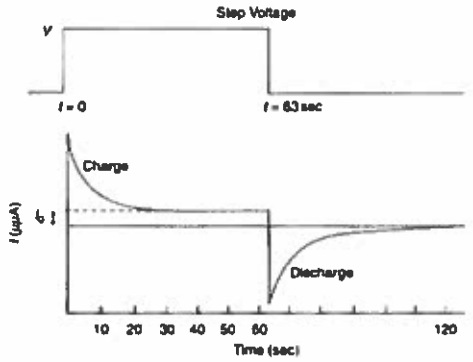

Fig. 4. Step voltage input and current output [7].

2.2.2. Frequency Domain Approach

We mainly measure the dielectric constant at various frequencies of alternating excitation fields. No material is free of dielectric losses and therefore no material is free of absorption and dispersion which reflects that no material is frequency independent $\varepsilon_r^{'}$ and $\varepsilon_r^{''}$. Now, using Debye Equations for a varying electric field $F_m e^{j\omega t}$ we have the relationships as:

$$\varepsilon_r^{'} = \varepsilon_{r\infty} + \frac{\varepsilon_{rs} + \varepsilon_{r\infty}}{1+\omega^2\tau_0^2} \tag{9}$$

$$\varepsilon_r^{''} = \frac{(\varepsilon_{rs} - \varepsilon_{r\infty})\omega\tau_0}{1+\omega^2\tau_0^2} \tag{10}$$

$$\tan\delta = \varepsilon_r^{''}/\varepsilon_r^{'} = \frac{(\varepsilon_{rs} - \varepsilon_{r\infty})\omega\tau_0}{\varepsilon_{rs} + \varepsilon_{r\infty}\omega^2\tau_0^2} \tag{11}$$

From Eq.(s) 10 and 11 we get the parametric equations of circle in $\varepsilon_r^{'} - \varepsilon_r^{''}$, given as:

$$\begin{aligned} \frac{\varepsilon_r^{'} - \varepsilon_{r\infty}}{\varepsilon_{rs} - \varepsilon_{r\infty}} &= \frac{1}{1+\omega^2\tau_0^2} \\ \frac{\varepsilon_r^{''}}{\varepsilon_{rs} - \varepsilon_{r\infty}} &= \frac{\omega\tau_0}{1+\omega^2\tau_0^2} \end{aligned} \tag{12}$$

By eliminating $\omega\tau$ from eq. 12 we obtain,

$$\left(\varepsilon_r^{'} - \frac{\varepsilon_{rs} + \varepsilon_{r\infty}}{2}\right)^2 + \varepsilon_r^{''2} = \left(\frac{\varepsilon_{rs} - \varepsilon_{r\infty}}{2}\right)^2 \tag{13}$$

The circle of Eq. 13 over which $\varepsilon_r^{''}$ is positive has physical significance (a semicircle). This complex plot of $\varepsilon_r^{'} - \varepsilon_r^{''}$ defined as *Argand diagram* is shown in Fig. 6 in which frequency is not explicitly shown. The variation of $\varepsilon_r^{'}$ and $\varepsilon_r^{''}$ due to the variation of ω is shown in Fig. 5 which illustrates schematically the typical dispersion behavior for polarization in the relaxation regime. For simplicity, Eq.(s) 9, 10 and 11 are based on the following assumptions: the local field is the same as the applied field F; the conductivity of the materials is negligible; all dipoles have only one identical relaxation time τ_o. For more insight into Debye Equations for atmospheric ice and various forms see Mughal et. al. [8].

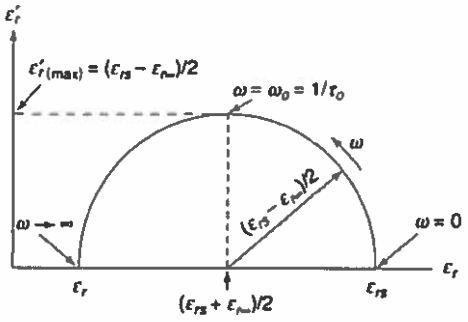

Fig. 5. Argand Diagram $\varepsilon_r^{'} - \varepsilon_r^{''}$.

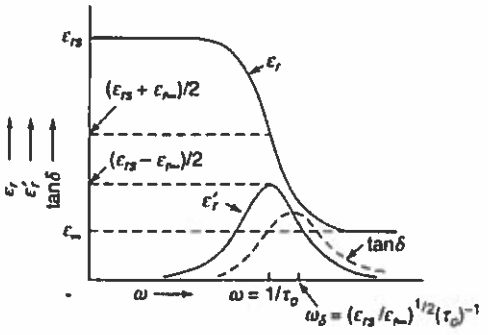

Fig. 6. Variation of $\varepsilon_r', \varepsilon_r'', \delta$ as a function of ω.

3. Capacitive Atmospheric Icing Sensors

Capacitive ice sensors generate an electric field to detect the presence of dielectric materials. Such electric field radiates outward around the probe and a dielectric material in close proximity of the field affects the measured capacitance, Mughal et. al. [6]. This attribute enables non-invasive measurements. In Sihvola et. al. [9], the results indicate that the complex dielectric constant is practically independent of the structure of snow. It is also mentioned that for dry snow, the dielectric constant is determined by the density and for wet snow, the imaginary part and the increase of the real part due to liquid water have the same volumetric wetness dependence. The static dielectric constants ε_{rs} of both polycrystalline and single crystals of ice have been carefully determined Auty [10]. Also, application electrical properties to the measurement of ice thickness, temperature, crystal orientations are presented in Evanes [11]. Weinstein [12], Kwadwo [13] and Jarvinen [14] proposed three different capacitive based ice detection methods, which are discussed in the following sections.

3.1. Capacitive Ice Sensor by Weinstein

This ice sensor proposed by Weinstein [12] as given in Fig. 7 can be used for the determination of the thickness of ice (22) on the outer surface (12) of an object independent of temperature and the composition of the ice (22). First capacitive gauge (16), second capacitive gauge (18), and the temperature gauge (20) are embedded in embedding material (14) located within a hollow portion of outer surface (12). First capacitive gauge (16), second capacitive gauge (18), and temperature gauge (20) are respectively connected to first capacitance measurement circuit (24), second capacitance measurement circuit (26), and temperature measuring circuit (28). The geometry of first and second capacitive gauge s (16) and (18) is such that the ratio of voltage outputs of first and second capacitive gauge s (24) and (26) is proportional to the thickness of ice (22), regardless of ice temperature or composition. This ratio is determined by offset and dividing circuit (29).

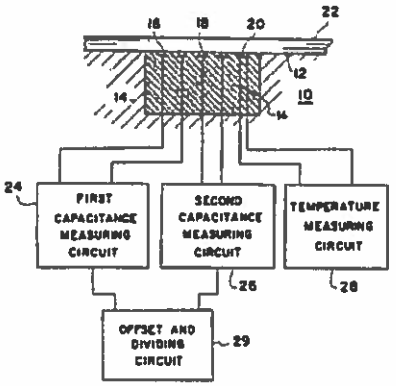

Fig. 7. Construction of Weinstein Ice Sensor.

In this sensor both first (16) and second capacitive gauge (18) are made from thin conductors with a thickness of approximately 0.001 of an inch. The first capacitance gauge (16) is connected to first capacitance measuring circuit (24) and second capacitance gauge (18) is connected to second capacitance measuring circuit (26) shown in Fig. 8. A dual timer LM556 (42), is used in an unstable mode to generate 7μs pulses at 1.5 kHz, for example, or pulses at any other similar frequencies, which are used to trigger a monostable timer (44). The timing capacitor of monostable timer (44) is gauge 16. The output from the monostable timer is converted by the low pass filter (46) to produce an output DC signal which is directly proportional to the capacitance of first capacitance gauge (16). First capacitance measuring circuit (24) and second capacitance measuring circuit (26) are connected to offset the dividing circuit (29). The output voltage V_{out} of this offset and dividing circuit (29) for ice conditions is determined by the relation,

$$V_{out} = \frac{(V - V_o)_2}{(V - V_o)_1}, \tag{14}$$

where V is the voltage output for the ice conditions and V_o is the initial voltage for no ice conditions. Subscripts (1) and (2) refer respectively to capacitive measurements from first capacitance measuring circuit (24) and second capacitance measurement circuit (26). V_{out} is independent of both temperature and ice decomposition since both effects results in identical scaling factors [15] resulting no changes in Eq.(s) 14. The variation of capacitance as a function of thickness is shown in Fig. 9.

In Fig. 9 output voltages from first and second capacitive measuring circuits (24) and (26) for various thickness of ice (22) formed on the outer surface (12) is shown. Curve (48) represents the output voltage V_1 from the first capacitance

measuring circuit (24) at a fixed temperature and ice impurity level. Also curve (50) represents the voltage output V_2 from the second capacitance measuring circuit (26). At a fixed configuration, both curves will vary with temperature change or ice impurity change. Also it can be seen that both curves do not go to zero output voltage even when the ice thickness is zero.

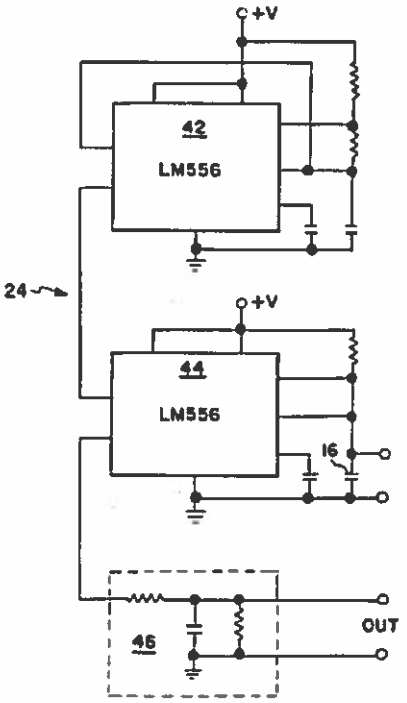

Fig. 8. Electrical schematic diagram of capacitance measuring circuit.

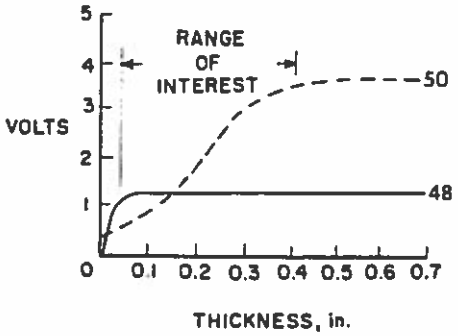

Fig. 9. Ratio of capacitance gauge as a function of thickness.

3.2. Atmospheric Icing Sensor by Kwadwo

Kwadwo [13] has used two-cylinder probes to act as a capacitive ice sensor, based on the principle that as ice accretes on two electrically charged parallel-arranged cylindrical probes, the measured capacitance increases, while the resistance decreases. As the super cooled water droplets collide with the cylindrical probes and stick on the surface, they freeze and ice begins to grow as shown in Fig. 11. The accreted ice affects the electric field generated by the electrically charged cylindrical probes resulting in an increase in the capacitance. At locations further from the inner region, i.e. along the circumference of the cylinders, the electric field lines are non-uniformly distributed, bulging out (instead of been parallel to each other), as one move away from the inner region. This non-uniformity of the electric field lines in these regions leads to a reduction in the electric field strength. This is known as fringing, which leads to decrease in capacitance. The electric field originating from the polarization charges on the surface of the ice partly shields the external electric field generated by the charged cylindrical probes leading to a reduction in the overall electric field. The overall voltage decreases simultaneously, because the electric field is directly proportional to the voltage. The resistance between the cylindrical probes is large at the start of the icing event because of the air gap between the cylinders. However, as ice builds up on the cylindrical probes, the air gap between the cylindrical probes decreases and the resistance begins to decrease exponentially. The rate of decrease is sensitive to the presence of water on the surface of the ice formed on the cylindrical probes and this phenomenon is used to distinguish between different types of ice.

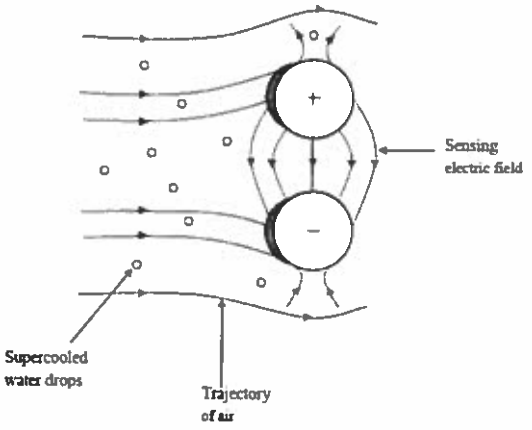

Fig. 10. Trajectory of supercooled water drops and air moving towards two cylindrical probes.

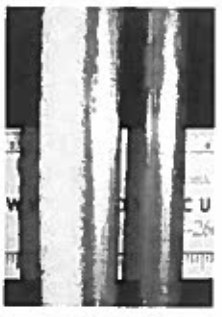

Fig. 11. Ice formation at the windward side of the cylindrical probes.

3.3. Atmospheric Icing Sensor by Jarvenin

In this sensor, Jarvinen [14] used the method for detecting the presence and the accretion of ice by first measuring the properties of the contaminant layer overlying the ice sensor. The contaminant layer's temperature, thermal conductivity and variation of total impedance versus ice sensor electrical excitation frequency are measured. The complex dielectric property subsystem monitors the dielectric property locus in dielectric space as the excitation frequency is varied from near dc to higher frequencies (using Cole-Cole plot) and compares the measured results for magnitude and shape with laboratory property data taken at the same temperature and stored in the processor. It doubles checks using external ice (based upon the complex dielectric measurements) sensor whether it is ice or rain water or deicing fluid or snow. If the measured results form a semicircular shaped locus of dielectric properties in complex dielectric space during the frequency scan and those measurements are also determined to be in agreement with on board stored laboratory ice data, ice is confirmed to be present. The presence of ice is also confirmed if a particular vector can be constructed from the measured data taken at a single preselected excitation frequency and found to have a vector angle in agreement with the vector angle from stored laboratory results taken at the same measurement conditions. In addition, complex dielectric measurement algorithms identify whether cracks, flaws or voids or increased electrical conductivity exist in the ice covering and sensor from their effects on the shape and size of the measured complex dielectric locus or from the length of the vector at the pre selected frequency. The presence of flaws, cracks or voids or enhanced electrical conductivity are determined from the values for the low frequency and high frequency intercepts and the value for diameter of the complex dielectric locus if these values are found to differ from those calculated for ice based on stored ice data. These differences, if found to exist, are used to correct the initially chosen ice thickness value based on the assumption of normal ice: ice with no flaws, cracks or voids or higher electrical conductivity, see Fig. 12. For more details on the mathematical principle of this type of sensing technique see Mugal et. al. [8].

Pure glaze ice in the temperature range from *0* to *-40 °C* has a thermal conductivity value in the range *2.4* to *2.6 W/mK*, rain water slightly above *0 °C* has a value of *0.6 W/mK* in the same units, air *0.023 W/mK* and a *50/50* mixture of deicing fluid is *0.41 W/mK*. The thermal conductivity of rime ice (density *0.38 gm/cm³*) has a thermal conductivity of *0.4 W/mK*. Thus the presence of glaze ice is easily determined by the substantial difference in thermal conductivity between it and all other possible contaminants. More details about this can be found in [15]. Dielectric values are used in addition to discriminate between rain water, deicing fluid and low density rime ice.

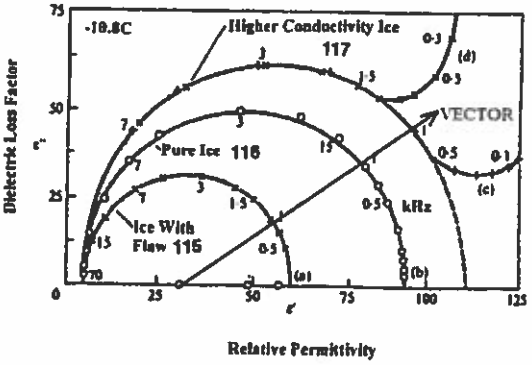

Fig. 12. Cole-Cole plot for pure ice, ice with flaw and ice with higher conductivity value [14].

Also this sensor uses *AD5933* high precision impedance converter system that combines an on board frequency generator with a *12 bit*, *1 MSPS*, *ADC*. The frequency generator allows an external complex impedance to be excited with a known frequency. The response signal from the impedance is sampled by the on board *ADC* and a discrete Fourier transform is processed by an on board DSP engine. The DFT algorithm returns a real and imaginary data word at each output frequency. *AD5933* chip measures total impedance magnitudes over the range from *100 Ω* to *10 MΩ* with a total system accuracy of *0.5 %*. The sweep frequency range of the chip normally covers the range from *1 kHz* to *100 kHz*. However by adding a clock dividing circuit we can lower the range to *10 Hz* to *20 kHz*. For this sensor this range is *40 Hz* to *40 kHz*.

3.3.1. From Impedance to Dielectric

It is explained in [16] that ice can may be replaced by an equivalent circuit as shown in Fig. 12. The total complex impedance Z of the circuit is given by

$$\frac{1}{Z}=\frac{1}{R_c}+\frac{1}{R_i+\frac{1}{j\omega C_i}}+j\omega C_a \tag{15}$$

Now if the ice is characterized by a capacitance *C*, then

$$\frac{1}{Z_c}=j\omega C=\frac{j\omega A\varepsilon_0\varepsilon_r}{L}, \tag{16}$$

where *L* is the thickness of ice, *A* is the surface area of block of ice and ε_0 is the permittivity of free space. Also we can write

$$\varepsilon_{ra}=\frac{L}{\varepsilon_0 A}(C_i+C_a),$$
$$\varepsilon_{re}=\frac{LC_a}{\varepsilon_0 A} \tag{17}$$

which is when substituted in eq. 16 then we have

$$\varepsilon_r = \frac{LC_1}{\varepsilon_0 A(1+j\omega\tau)} + \frac{LC_\infty}{\varepsilon_0 A}, \tag{18}$$

where $\tau = R_1C_1$ is the dielectric relaxation time of the circuit that is time taken for the voltage across the ice block to reach $1\text{-}e^{-1} = 0.63$ of its final value when a step voltage is applied. Similarly we can also write the complex permittivity as

$$\varepsilon' = \frac{L}{\varepsilon_0 A}\left(\frac{C_1}{1+\omega^2\tau^2} + C_\infty\right)$$
$$\varepsilon'' = \frac{L}{\varepsilon_0 A}\left(\frac{\omega\tau C_1}{1+\omega^2\tau^2}\right) \tag{19}$$

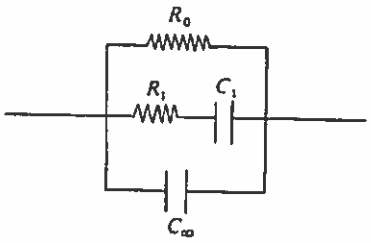

Fig. 13. Equivalent circuit for ice [16].

3.3.2. How to Measure Thickness

In operation the ice detection system knowing the type of ice from impedance, thermal conductivity and or dielectric measurements, then takes the measured impedance value and converts it to a thickness after interpolation to the measured local temperature should that temperature not be an exact temperature match with the look up data. The contaminants layer temperature, thermal conductivity and variation of total impedance versus ice sensor electrical excitation frequency are measured and the total impedance data is also converted to show the complex dielectric properties of the overlying layer. The measured properties and the complex dielectric properties are then used first to differentiate between ice, rain water, deicer fluid or snow overlying the ice sensor and then used to differentiate between glaze and rime ice by comparing the results with laboratory measured ice data stored in computer memory collocated with the ice sensor. The presence of ice is confirmed by a measured thermal conductivity value in agreement with that of ice and also confirmed if its complex dielectric locus exhibits a semicircular shape with values for the diameter of the complex dielectric locus and for its low frequency and high frequency intercepts with the ordinary relative permittivity axis in near agreement with similar results calculated form the stored laboratory measured ice data. A second possible simplified means for confirming the presence of ice is also provided based on demonstrating that the magnitude and angular inclination of a vector from a point on the ordinary relative permittivity axis near the high frequency end of the complex dielectric locus, the vector starting near the locus.

4. Conclusion and Future Work

The mere existence of a permanent dipole moment in water provides structural information about the molecule. It is found that the dielectric variations in different types of ice can be very effective in finding the parameters such as ice type, ice thickness and icing rate. The patent of Jaravinen [14] can be considered as a benchmark as it is able to sense all the above parameters, hence the direct approach mentioned by Homola et. al. [3] is able to deliver maximum information. Also due to the variation in response of ice and snow by varying the electrical field; the application of Cole-Cole Diagram for complex dielectric constant of snow and ice is adequately proved. A simulation study [17] and analytical study [8] on the capacitive variations of atmospheric ice is carried out to compare the numerical and theoretical results with the experimental variations. These results can further be utilized/validated for the determination of atmospheric ice type and measurement of its rate and thickness. A hybrid measurement technique may also be considered in future for robust results.

Acknowledgements

The work reported in this paper was partially funded by the Research Council of Norway, project no. 195153/160 and partially by the consortium of the ColdTech project - Sustainable Cold Climate Technology. Also I appreciate the support of Norwegian PhD Network on Nanotechnology for Microsystems, contract no. 190086/S10 for their financial and technical support.

References

[1]. Foder, M. H. ISO 12494 - Atmospheric icing on structures and how to use it, in *Proceedings of the 11th International Offshore and Polar Engineering Conference*, Norway, 2001.

[2]. Fikke, S., Atmospheric icing on structures, measurement and data collection on icing, state of the art, *MeteoSwiss*, 2006, p. 110.

[3]. Homola, M. C., P. J. Nicklasson, and P. A. Sundsbo, Ice sensors for wind turbines, *Cold Regions Science and Technology*, 2006, 46, p. 125-131.

[4]. Craig, D. F. and D. B. Craig, An investigation of icing events on haecket hill, in *Proceedings of the Boreas III Conference*, Finland, 1995.

[5]. Seifert, H., Technical requirements for rotor blades operating in cold climates, in *Proceedings of the Boreas II Conference*, Pyhatunturi, Finland, 2003.

[6]. Mughal, U. N. and M. S. Virk, Review of Atmospheric Icing Sensors.
[7]. Kao, K. C., Dielectric phenomena in solids, *Academic Press*, 1 edition (March 25, 2004).
[8]. Mughal, U. N., M. S. Virk, and M. Y. Mustafa, Dielectric based sensing of atmospheric ice, in *Proceedings of the 38th International Conference on Application of Mathematics in Engineering and Economics*, Sozopol, Bulgaria, AIP, 2012.
[9]. Sihvola, A., E. Nyfors, and M. Tiuri, Mixing formulae and experimental results for the dielectric constant of snow, *Journal of Glaciology*, 31, 108, 1985, pp.163-170.
[10]. Auty, R. P., Dielectric Constants of Solid H_2O and D_2O, *Brown University*, 1951.
[11]. Evans, S., Dielectric properties of ice and snow - a review, *Journal of Glaciology*, 5, 1965, pp. 773-792.
[12]. Weinstein, L. M., Ice Sensor, US Patent No. 4766369, 1988.
[13]. Owusu, K. P., Capacitive probe for ice detection and accretion rate measurement: proof of concept, *University of Mannitoba*, Mannitoba, 2010.
[14]. Jarvinen, P. O., Total impedience and complex dielectric property ice detection system, 2008.
[15]. Coles, W. D., Experimental determination of thermal conductivity of low density ice, *Technical Notes*, 3143, *Wash. DC NACA*, 1954.
[16]. Hobbs, P. V., Ice Physics, *Oxford University Press*, 2010.
[17]. Mughal, U. N. and M. S. Virk, A Numerical Comparison of Dielectric based Measurement of tmospheric Ice Using Comsol, in *Comsol Multiphysics*, Milan, Italy, 2012.